An implicit implementation of surface tension in finite volume models for two-phase flows

M. Raessi,* M. Bussmann, and J. Mostaghimi
Centre for Advanced Coating Technologies,
Department of Mechanical and Industrial Engineering,
University of Toronto

Abstract

We present an implicit implementation of surface tension in finite volume models for two-phase flows. Using the implicit model, the surface tension time step restriction, which is often the strictest one, can be exceeded without destabilizing the solution. The surface tension force in the implicit model consists of an explicit part, which is the regular continuum surface force (CSF), and an implicit part which represents the diffusion of velocities induced by surface tension on an interface between two fluids. The surface tension force is applied on velocity field by solving a system of equations iteratively. Since the equations are solved only near an interface, the computational time spent on the iterative procedure is insignificant.

---

*Corresponding Author. Email: mraessi@mie.utoronto.ca

Introduction

The continuum surface force (CSF) model [1], developed a decade ago, has been widely used for implementing surface tension forces in interfacial flow models. The CSF model is explicit, and thus for numerical stability, the timestep size Δt must satisfy the following condition:

$$\Delta t \leq \Delta t_{ST} = \sqrt{\frac{\overline{\rho}(\Delta x)^3}{2\pi\sigma}} \qquad (1)$$

where $\overline{\rho}$ is the average density of two phases, σ is the surface tension, and Δx is the mesh size. This condition imposes a stringent constraint on Δt, especially if surface tension is a dominant force.

If the viscous effects are also modelled by an explicit approach, then Δt must also satisfy the following condition:

$$\Delta t \leq \Delta t_{vis.} = \frac{\rho(\Delta x)^2}{2\mu} \qquad (2)$$

where μ is fluid viscosity.

In addition to the above restrictions, Δt must satisfy the Courant-Friedrichs-Lewy (CFL) condition which results from using an explicit time-marching scheme for discretizing the convective term:

$$\Delta t_{CFL} \leq \frac{\Delta x}{u} \qquad (3)$$

where u represents velocity.

To compare these timestep restrictions, consider a 100 micron water droplet moving at 1 m/s, discretized by 20 cells per radius ($\Delta x = 2.5 \times 10^{-6}$ m). The timestep restrictions are

$$\begin{aligned}
\Delta t \leq & \quad \Delta t_{ST} = 2.5 \times 10^{-7}\,\text{s} \\
\Delta t \leq & \quad \Delta t_{vis.} = 8 \times 10^{-6}\,\text{s} \\
\Delta t \leq & \quad \Delta t_{CFL} = 2.5 \times 10^{-6}\,\text{s}
\end{aligned}$$

As we see, the timestep restriction due to surface tension is an order of magnitude smaller than the others. If this restriction is removed, or at least mitigated, then time-marching can be done at larger timesteps, and hence simulation run times can be reduced significantly. In the above example, by removing the surface tension timestep restriction, one could run simulations 10 times faster.

Hysing [2] presented an implicit approach to the CSF model in a finite-element context, in which Δt_{ST} is exceeded by at least a factor of 10. In this paper, we present an implementation of Hysing's model for a finite-volume method. We do this in the context of a volume-of-fluid (VOF)-based model; however, the implementation presented here could also be extended to models which employ other interface tracking techniques, such as the level set method.

Mathematical fundamentals

Consider a two-phase flow where fluids are immiscible and both incompressible. The governing equations are conservation of mass and momentum:

$$\nabla \cdot \vec{U} = 0 \qquad (4)$$

$$\begin{aligned}
\frac{\partial\left(\rho\vec{U}\right)}{\partial t} + \nabla \cdot \left(\rho\vec{U}\vec{U}\right) = -\nabla P + \\
\nabla \cdot \left(\mu\left(\nabla\vec{U} + \nabla^T\vec{U}\right)\right) + \vec{F}_{ST} + \vec{F}_B
\end{aligned} \qquad (5)$$

where $\vec{U}$ is the velocity, P the pressure, $\vec{F}_{ST}$ the surface tension force, and $\vec{F}_B$ any body forces, such as gravity.

Using a first-order scheme to discretize the temporal derivative in Eq. (5), and employing a two-step projection method, we solve Eq. (5) by splitting it into predictor and corrector steps:

$$\begin{aligned}
\frac{\rho^{n+1}\vec{U}^* - \rho^n\vec{U}^n}{\Delta t} = \\
-\nabla \cdot \left(\rho\vec{U}\vec{U}\right)^n + \nabla \cdot \left(\mu\left(\nabla\vec{U} + \nabla^T\vec{U}\right)\right)^n + \\
\vec{F}_B^n + \vec{F}_{ST}^{n+1}
\end{aligned} \qquad (6)$$

$$\frac{\rho^{n+1}\vec{U}^{n+1} - \rho^{n+1}\vec{U}^*}{\Delta t} = -\nabla p^{n+1} \qquad (7)$$

where superscripts n and $n+1$ denote the current and next time levels, and * represents an interim level.

In the CSF formulation [1],

$$\vec{F}_{ST} = \sigma\kappa\hat{n}\delta_\Gamma \qquad (8)$$

where κ is interface curvature, $\hat{n}$ a unit normal vector to the interface, and δ_Γ the Dirac delta function.

Following [2], an identity mapping, denoted by id_Γ is defined on an interface Γ as

$$id_\Gamma = \vec{x}|_\Gamma = \vec{x}\delta_\Gamma$$

where $\vec{x}$ denotes the position vector. From differential geometry, we can show

$$\underline{\Delta}id_\Gamma = \kappa\hat{n} \qquad (9)$$

where $\underline{\Delta}$ is the tangential (or surface) Laplacian operator also known as the Laplace-Beltrami operator (see Appendix). Thus, $\vec{F}_{ST}$ becomes

$$\vec{F}_{ST} = \sigma\left(\underline{\Delta}id_\Gamma\right)\delta_\Gamma \qquad (10)$$

and the surface tension term in Eq. (5) can be written as

$$\vec{F}_{ST}^{n+1} = \sigma \left(\underline{\Delta} i d_{\Gamma}^{n+1} \right) \delta_{\Gamma} \qquad (11)$$

where id_{Γ}^{n+1} denotes the interface location at time $n+1$.

Following [2, 3], we use a backward Euler scheme to approximate id_{Γ}^{n+1} as

$$id_{\Gamma}^{n+1} = id_{\Gamma}^{n} + \Delta t \vec{U}^{n+1} \qquad (12)$$

which is analogous to

$$\vec{x}|_{\Gamma}^{n+1} = \vec{x}|_{\Gamma}^{n} + \Delta t \vec{U}^{n+1} \qquad (13)$$

We also consider the following approximation where the Crank-Nicolson scheme is used

$$id_{\Gamma}^{n+1} = id_{\Gamma}^{n} + \frac{\Delta t}{2} \left(\vec{U}^{n} + \vec{U}^{n+1} \right) \qquad (14)$$

Substituting Eqs. (12) and (14) into Eq. (11) and rearranging, we obtain

$$\vec{F}_{ST}^{n+1} = \sigma(\kappa \hat{n})^{n} \delta_{\Gamma} + \sigma \Delta t (\underline{\Delta} \vec{U}^{n+1}) \delta_{\Gamma} \qquad (15)$$

and

$$\vec{F}_{ST}^{n+1} = \sigma(\kappa \hat{n})^{n} \delta_{\Gamma} + \frac{\sigma \Delta t}{2} \left(\underline{\Delta} \vec{U}^{n} + \underline{\Delta} \vec{U}^{n+1} \right) \delta_{\Gamma} \quad (16)$$

The term $\sigma(\kappa \hat{n})^{n} \delta_{\Gamma}$ in Eqs. (15) and (16) is the regular CSF force (see Eq. (8)), and the additional term (see Appendix for $\underline{\Delta} \vec{U}$) represents diffusion of velocities induced by surface tension force on an interface. Note that as Δt tends to zero, the diffusive term vanishes, implying that as Δt decreases, the implicit implementation asymptotes to the familiar explicit implementation of the CSF model.

We use both forms of $\vec{F}_{ST}^{n+1}$, presented in Eqs. (15) and (16), in Eq. (6) and study the results. Rewriting Eq. (6) as

$$\rho^{n+1} \vec{U}^{*} = \widetilde{\rho \vec{U}} + \Delta t \vec{F}_{ST}^{n+1} \qquad (17)$$

where

$$\widetilde{\rho \vec{U}} = \rho^{n} \vec{U}^{n} + \Delta t \Big[-\nabla \cdot \left(\rho \vec{U} \vec{U} \right)^{n} + \\ \nabla \cdot \left(\mu \left(\nabla \vec{U} + \nabla^{T} \vec{U} \right) \right)^{n} + \vec{F}_{B}^{n} \Big] (18)$$

we first use the expression given in Eq. (15) for $\vec{F}_{ST}^{n+1}$ and substitute it into Eq. (17):

$$\rho^{n+1} \vec{U}^{*} = \widetilde{\rho \vec{U}} + \sigma \Delta t (\kappa \hat{n})^{n} \delta_{\Gamma} + \sigma (\Delta t)^{2} (\underline{\Delta} \vec{U}^{*}) \delta_{\Gamma} \quad (19)$$

In two-dimensional (2D) Cartesian coordinates, where we define $\vec{U} = (u, v)$ and $\hat{n} = (n_{1}, n_{2})$, and

using Eq. (A-12) for $\underline{\Delta} \vec{U}^{*}$, we obtain the following equation for applying surface tension on the u-component of velocity:

$$\rho^{n+1} u^{*} = \widetilde{\rho u} + \sigma \Delta t (\kappa n_{1})^{n} \delta_{\Gamma} + \\ \sigma (\Delta t)^{2} \Big[n_{2}^{2} u_{xx}^{*} + n_{1}^{2} u_{yy}^{*} - 2 n_{1} n_{2} u_{xy}^{*} - \\ (n_{1} u_{x}^{*} + n_{2} u_{y}^{*}) \big(n_{2}^{2} n_{1x} + n_{1}^{2} n_{2y} - \\ n_{1} n_{2} (n_{1y} + n_{2x}) \big) \Big] \delta_{\Gamma} \qquad (20)$$

where the subscripts x and y denote derivatives with respect to x and y, respectively, and $\widetilde{\rho u}$ is the x-component of Eq. (18). Similarly, for the v-component of $\vec{U}$, we have

$$\rho^{n+1} v^{*} = \widetilde{\rho v} + \sigma \Delta t (\kappa n_{2})^{n} \delta_{\Gamma} + \\ \sigma (\Delta t)^{2} \Big[n_{2}^{2} v_{xx}^{*} + n_{1}^{2} v_{yy}^{*} - 2 n_{1} n_{2} v_{xy}^{*} - \\ (n_{1} v_{x}^{*} + n_{2} v_{y}^{*}) \big(n_{2}^{2} n_{1x} + n_{1}^{2} n_{2y} - \\ n_{1} n_{2} (n_{1y} + n_{2x}) \big) \Big] \delta_{\Gamma} \qquad (21)$$

To apply surface tension on the velocity field, these equations are solved for u^{*} and v^{*} at each timestep by solving systems of algebraic equations.

Substituting Eq. (16) into Eq. (17) then yields

$$\rho^{n+1} \vec{U}^{*} = \widetilde{\rho \vec{U}} + \sigma \Delta t (\kappa \hat{n})^{n} \delta_{\Gamma} + \\ \frac{\sigma (\Delta t)^{2}}{2} (\underline{\Delta} \vec{U}^{n} + \underline{\Delta} \vec{U}^{*}) \delta_{\Gamma} \qquad (22)$$

which can also be written in terms of u and v, similar to Eqs. (20) and (21).

Numerical methodology

Using a two-step projection method, Eqs. (4) and (5) are solved in 2D Cartesian coordinates. In the predictor step (Eq. (6)), an interim velocity $\vec{U}^{*}$ is calculated by considering convective, viscous terms, surface tension and body forces. Then, in the corrector step (Eq. (7)), Eq. (4) at time level $n+1$ is employed to yield an implicit equation for pressure:

$$\frac{1}{\Delta t} \left(-\nabla \cdot \vec{U}^{*} \right) = -\nabla \cdot \nabla p^{n+1} \qquad (23)$$

A solution for pressure is obtained at each timestep from Eq. (23), and finally the new velocity field $\vec{U}^{n+1}$ is evaluated via Eq. (7).

A collocated arrangement of variables is used here, where pressure and velocities are defined at cell-centers. By incorporating a consistent mass and momentum advection scheme [4], the flow model can simulate high density ratio flows. In addition to the implicit implementation of surface tension, i.e. the formulations presented in Eqs. (15) and (16), we also

consider the standard CSF [1] and the consistent CSF [5] models for comparison.

We use the "coupled level set and volume-of-fluid" (CLSVOF) method of Son and Hur [6] for this study. In this method, the interface is represented by a smooth level set (LS) function [7, 8] denoted by ϕ. For a domain Ω, ϕ is defined as a signed distance function to the boundary (interface) $\partial\Omega$

$$|\phi(\vec{x})| = \min(|\vec{x} - \vec{x_I}|) \quad \text{for all} \quad \vec{x_I} \in \partial\Omega \quad (24)$$

implying that $\phi(\vec{x}) = 0$ on $\partial\Omega$. Choosing ϕ to be positive inside Ω, we then have

$$\phi(\vec{x}) = \begin{cases} > 0, \vec{x} \in \Omega \\ 0, \quad \vec{x} \in \partial\Omega \\ < 0, \vec{x} \notin \Omega \end{cases} \quad (25)$$

The unit normal vector and curvature at any point on the interface are calculated from ϕ by

$$\hat{n} = \frac{\nabla\phi}{|\nabla\phi|} \quad (26)$$

and

$$\kappa = -\nabla \cdot \left(\frac{\nabla\phi}{|\nabla\phi|} \right) \quad (27)$$

The motion of the interface is defined by the following advection equation

$$\frac{\partial\phi}{\partial t} + \vec{U} \cdot \nabla\phi = 0 \quad (28)$$

When ϕ is advected, the $\phi = 0$ contour moves at the correct velocity and properly represents the interface; however, contours of $\phi \neq 0$ do not necessarily remain distance functions. This can result in an irregular ϕ field that in turn leads to problems with mass conservation. To rectify this problem reinitialization methods have been developed, which adjust ϕ back to a signed distance function without changing the $\phi = 0$ contour.

In the CLSVOF method, to reinitialize ϕ, the LS function is coupled with the VOF function. The VOF function, a scalar color function denoted by f, is defined as

$$f(\vec{x}) = \begin{cases} 1, \vec{x} \in \text{fluid1} \\ 0, \vec{x} \in \text{fluid2} \end{cases} \quad (29)$$

to represent fluid 1 in a two-phase system. The VOF function is advected by

$$\frac{\partial f}{\partial t} + \vec{U} \cdot \nabla f = 0 \quad (30)$$

After advecting ϕ and f from time n to $n+1$, the interface, approximated as piecewise linear, is then reconstructed from f^{n+1} using the interface normal vectors calculated from ϕ^{n+1}. ϕ is then reinitialized by calculating the distance between any cell center (where ϕ is defined) and the VOF interface.

The CLSVOF method achieves exact mass conservation if it is based on an exactly-conservative VOF approach. Here, the VOF function is advected by the method of Youngs [9], which is volume conserving. For the level set function ϕ, the spatial derivatives in Eq. (28) were discretized using a second-order accurate, essentially nonoscillatory (ENO) scheme and the forward Euler scheme was used to discretize the temporal derivative.

Results

Static drop in the absence of gravity

Consider a drop of fluid 1 with a radius of 0.25 centered at (0.5,0.5) in a 1×1 domain filled with fluid 2, in the absence of gravity. $\rho_1 = \rho_2 = 1000$, $\mu_1 = \mu_2 = 5 \times 10^{-2}$, $\sigma = 0.1$. $\Delta x = \Delta y = 1/128$. According to the surface tension and viscous timestep restrictions (Eqs. (1) and (2)), $\Delta t \leq \Delta t_{ST} = 0.03$ and $\Delta t \leq \Delta t_{vis.} = 0.61$.

To model the flow, we first used the standard and consistent CSF models [1, 5] and ran the simulation to $t = 90$ with $\Delta t = 0.015$. Table 1 shows the maximum and average magnitudes of dimensionless spurious currents $\vec{U}\mu/\sigma$ at $t = 90$, as well as the pressure jumps. ΔP_{total} denotes the difference between average pressures in the $r \leq R$ and $r > R$ regions, $\Delta P_{partial}$ represents the difference between average pressures in the $r \leq R/2$ and $r > 3R/2$ regions (to avoid the transition region around the interface), and ΔP_{max} is the difference between the maximum and minimum pressures in the domain. $\Delta P_{exact} = 0.4$. Note that the consistent CSF model yields smaller spurious currents. Also, the pressure jumps predicted by the standard and consistent CSF models are the same except for ΔP_{max}.

Note that when explicit surface tensions models are used it is possible to use timesteps up to $2\Delta t_{ST}$ and still obtain stable solutions in some cases. In fact, the way the surface tension timestep constraint was devised [1] allows for this. We successfully ran the above test with $\Delta t = 2\Delta t_{ST}$ using the consistent CSF model. However, when $\Delta t > 2\Delta t_{ST}$, the explicit surface tension models failed, as expected. For example, when the standard or consistent CSF models were used with $\Delta t = 6\Delta t_{ST}$, the solution became unstable after only eight or four timesteps, respectively. In this case, velocities induced by surface tension violated the CFL condition.

Next, we ran the same simulation but with the implicit implementation of surface tension (Eqs. (15)

and (16)). This time we used a range of timesteps: $\Delta t = 0.015$, 0.03, 0.06, 0.12, and 0.18, and exceeded Δt_{ST}. The solution was stable even when $\Delta t = 0.18 = 6\Delta t_{ST}$. The maximum and average magnitudes of dimensionless spurious currents at $t = 90$ are presented in Table 2 for both formulations.

Comparing the results at $\Delta t = 0.015$ with the ones from the explicit models, it can be seen that the consistent CSF model produces the smallest spurious currents, and that the magnitude of maximum spurious currents generated by the implicit models are smaller than those of the standard CSF model. However, the implicit models yield average spurious currents that are greater than those of the standard CSF model. This can be explained by considering Figure 1, which shows the spurious currents induced in the flow at $t = 90$, using different surface tension models. When the standard CSF model is used, the spurious currents, shown in Figure 1(c), are very large on the interface but quite small off the interface, making the average magnitude of currents small. When implicit models are used (Figures 1(a) and (b)), the currents are not as large as in the standard CSF result, but they are stronger far from the interface. Thus, the average magnitude of the spurious currents is larger when the implicit model is used. Figure 1(d) shows the consistent CSF model results magnified six times; as can be seen, spurious currents are larger on the interface and inside the drop, than outside.

As well, we notice that when the implicit models are used the pressure jumps decrease as Δt increases. This is less severe when the Crank-Nicolson scheme is used. We found that the reason lies in the left-hand side of Eq. (23), i.e. the source term of the pressure equation. As Δt increases, $\vec{U}$ and effectively $\nabla \cdot \vec{U}$ increase quite linearly for $\Delta t \leq 2\Delta t_{ST} = 0.06$. However, as we saw in Table (2), when $\Delta t > 0.06$, $\vec{U}$ starts to asymptote, and hence the source term of the pressure equation becomes smaller, which causes the loss in pressure jump.

Note that at the same timestep, run times are very close among the implicit and explicit surface tension models. For example, when $\Delta t = 0.015$, run times of the standard CSF, consistent CSF, and implicit models (both formulations) are 175, 170, and 177 minutes, respectively, suggesting that the time spent on the iterative solution of Eq. (19) or (22) is insignificant. This is because these equations are solved only in cells near an interface, where surface tension effects are present.

Buoyancy-driven flow

Consider a bubble of fluid 1 in a 1×2 container filled with fluid 2. The radius of the bubble is 0.1, and it is positioned at (0.5,0.5). $\rho_1 = 500$, $\rho_2 = 1000$, $\mu_1 = \mu_2 = 10^{-2}$, $\sigma = 0.1$, $g = -9.81 \times 10^{-3}$, and $\Delta x = \Delta y = 1/128$. The surface tension and viscous timestep restrictions are $\Delta t \leq \Delta t_{ST} = 0.024$ and $\Delta t \leq \Delta t_{vis.} = 1.53$.

We simulated the rise of the bubble due to buoyancy effects by using the implicit surface tension models, as well as the standard and consistent CSF models. Figure 2 illustrates bubble shapes at $t = 0$, 18, and 36 when $\Delta t = 0.006$ and 0.012, and Figure 3 displays results from the implicit methods at $\Delta t = 0.12 = 5\Delta t_{ST}$.

At $\Delta t = 0.006$, the results of the implicit models and the standard CSF are quite similar. This is expected because at small timesteps, the diffusive terms in Eqs. (15) and (16) approach zero; hence the implicit models are almost identical to the standard CSF. Note that when consistent CSF is used, the interface shape at $t = 36$ is different than the one predicted by the other models. This is probably due to the consistent treatment of surface tension and pressure, which yields a more accurate representation of surface tension forces.

With $\Delta t = 0.012$, results of the implicit models are almost identical but they differ in terms of interface shape from that of the explicit models. Note that interface shapes predicted by explicit models are different, too, probably due to the same reason discussed above. The height of bubble, however, is almost the same for all models.

Finally, when $\Delta t = 0.12$, at which the explicit models are unstable, the implicit models yield slightly different interface shapes. Note that at $\Delta t = 0.12$, the magnitudes of the diffusive terms in Eqs. (15) and (16) are significant and also different, which result in different surface tension forces and interface shapes. Furthermore, at this timestep, the height of the bubble is calculated to be slightly lower than that obtained at smaller timesteps. The differences between drop shapes and heights predicted by the implicit and explicit surface tension models, which become more obvious when the timestep is large, may be related to the loss in pressure jump in the static drop presented earlier. This issue needs to be further investigated and rectified.

Summary

The surface tension timestep restriction which is imposed by the explicit standard and consistent CSF models [1, 5] is stringent, especially when surface tension is a dominant force. Hysing [2] has

presented an implicit surface tension method in a finite-element context, where the timestep restriction is mitigated significantly. Here, we presented a method for implementing Hysing's model in interfacial flow models which are based on finite-volume method. The solution of velocity induced by surface tension involves an iterative procedure on cells near an interface; hence the computational time spent on the iterative procedure is insignificant. It was shown that the surface tension timestep restriction can be exceeded by at least a factor of 5 using implicit models, without destabilizing the numerical solutions.

Appendix

Tangential gradient

The tangential gradient of a scalar function f is defined as

$$\underline{\nabla} f = \nabla f - (\hat{n} \cdot \nabla f)\,\hat{n} \tag{A-1}$$

where ∇ denotes the regular gradient, and $\hat{n}$ is the unit normal vector of the surface on which the tangential gradient is calculated. The tangential gradient is then the directional derivative of f in the direction tangent to a surface.

In two-dimensional (2D) Cartesian coordinates, where $f = f(x, y)$ and $\hat{n} = n_1\hat{i} + n_2\hat{j}$, the tangential gradient is

$$\underline{\nabla} f = (f_x\hat{i} + f_y\hat{j}) - (n_1 f_x + n_2 f_y)(n_1\hat{i} + n_2\hat{j}) \tag{A-2}$$

or

$$\underline{\nabla} f = \Big(f_x - n_1(n_1 f_x + n_2 f_y)\Big)\hat{i} + \\ \Big(f_y - n_2(n_1 f_x + n_2 f_y)\Big)\hat{j} \tag{A-3}$$

where subscripts x and y denote differentiation with respect to x and y, respectively.

Tangential Laplacian

The tangential Laplacian or Laplace-Beltrami operator of f is defined as

$$\underline{\Delta} f = \underline{\nabla} \cdot \underline{\nabla} f \\ = \nabla \cdot \underline{\nabla} f - (\hat{n} \cdot \nabla)(\underline{\nabla} f) \cdot \hat{n} \tag{A-4}$$

In 2D, the first term in Eq. (A-4) is

$$\nabla \cdot \underline{\nabla} f = \nabla \cdot \left(\Big(f_x - n_1 \underbrace{(n_1 f_x + n_2 f_y)}_{=A}\Big)\hat{i} + \right. \\ \left. \Big(f_y - n_2(n_1 f_x + n_2 f_y)\Big)\hat{j} \right) \\ = f_{xx} - n_{1x}A - n_1 A_x + \\ f_{yy} - n_{2y}A - n_2 A_y \tag{A-5}$$

In the second term of Eq. (A-4)

$$(\hat{n} \cdot \nabla)(\underline{\nabla} f) = n_1 \tfrac{\partial}{\partial x}(f_x - n_1 A)\hat{i} + \\ n_2 \tfrac{\partial}{\partial y}(f_x - n_1 A)\hat{i} + \\ n_1 \tfrac{\partial}{\partial x}(f_y - n_2 A)\hat{j} + \\ n_2 \tfrac{\partial}{\partial y}(f_y - n_2 A)\hat{j} \\ = \Big(n_1 f_{xx} - n_1(n_{1x}A + n_1 A_x) + \\ n_2 f_{xy} - n_2(n_{1y}A + n_1 A_y)\Big)\hat{i} \\ + \\ \Big(n_1 f_{xy} - n_1(n_{2x}A + n_2 A_x) + \\ n_2 f_{yy} - n_2(n_{2y}A + n_2 A_y)\Big)\hat{j} \tag{A-6}$$

and so,

$$(\hat{n} \cdot \nabla)(\underline{\nabla} f) \cdot \hat{n} = n_1^2 f_{xx} - n_1^2(n_{1x}A + n_1 A_x) + \\ n_1 n_2 f_{xy} - n_1 n_2(n_{1y}A + n_1 A_y) + \\ n_1 n_2 f_{xy} - n_1 n_2(n_{2x}A + n_2 A_x) + \\ n_2^2 f_{yy} - n_2^2(n_{2y}A + n_2 A_y) \tag{A-7}$$

Combining, Eqs. (A-5) and (A-7):

$$\underline{\Delta} f = f_{xx}(1 - n_1^2) + f_{yy}(1 - n_2^2) - 2n_1 n_2 f_{xy} - \\ n_{1x}A(1 - n_1^2) - n_1 A_x(1 - n_1^2 - n_2^2) - \\ n_{2y}A(1 - n_2^2) - n_2 A_y(1 - n_1^2 - n_2^2) + \\ n_1 n_2 A(n_{2x} + n_{1y}) \tag{A-8}$$

or

$$\underline{\Delta} f = n_2^2 f_{xx} + n_1^2 f_{yy} - 2n_1 n_2 f_{xy} - (n_1 f_x + \\ n_2 f_y)\Big(n_1^2 n_{2y} + n_2^2 n_{1x} - n_1 n_2(n_{2x} + n_{1y})\Big) \tag{A-9}$$

Tangential gradient and tangential Laplacian of a vector

Consider a vector quantity $\vec{U}$ in 2D where

$$\vec{U} = u\hat{i} + v\hat{j} \tag{A-10}$$

On a surface with unit normal vector $\hat{n} = n_1\hat{i} + n_2\hat{j}$, the tangential gradient and tangential Laplacian of $\vec{U}$ are

$$\underline{\nabla}\vec{U} = \begin{bmatrix} u_x & u_y \\ v_x & v_y \end{bmatrix} - \\ \begin{bmatrix} n_1(n_1 u_x + n_2 u_y) & n_2(n_1 u_x + n_2 u_y) \\ n_1(n_1 v_x + n_2 v_y) & n_2(n_1 v_x + n_2 v_y) \end{bmatrix} \tag{A-11}$$

and

$$\underline{\Delta}\vec{U} = \begin{bmatrix} n_2^2 u_{xx} + n_1^2 u_{yy} - 2n_1 n_2 u_{xy} - (n_1 u_x + \\ n_2 u_y)\Big(n_2^2 n_{1x} + n_1^2 n_{2y} - n_1 n_2 (n_{1y} + n_{2x})\Big) \\ \\ n_2^2 v_{xx} + n_1^2 v_{yy} - 2n_1 n_2 v_{xy} - (n_1 v_x + \\ n_2 v_y)\Big(n_2^2 n_{1x} + n_1^2 n_{2y} - n_1 n_2 (n_{1y} + n_{2x})\Big) \end{bmatrix}$$

(A-12)

References

[1] J. U. Brackbill, D. B. Kothe, and C. Zemach. *J. Comput. Phys.*, 100:335–354, 1992.

[2] S. Hysing. *Int. J. Numer. Meth. Fluids*, 51:659–672, 2006.

[3] E. Bänsch. *Numer. Math.*, 88(2):203–235, 2001.

[4] M. Bussmann, D. B. Kothe, and J. M. Sicilian. *Proceedings of ASME 2002 Fluids Engineering Division Summer Meeting*, Montreal, Canada, 2002.

[5] M. M. Francois, S. J. Cummins, E. D. Dendy, D. B. Kothe, J. M. Sicilian, and M. W. Williams. *J. Comput. Phys.*, 213(1):141–173, 2006.

[6] G. Son and N. Hur. *Numer. Heat Transfer, Part B*, 42:523–542, 2002.

[7] S. Osher and J. A. Sethian. *J. Comput. Phys.*, 79:12–49, 1988.

[8] S. Osher and R. Fedkiw. *Level Set Methods and Dynamic Implicit Surfaces.* Springer-Verlag, New York, 2003.

[9] D. L. Youngs. In K. W. Morton and M. J. Baines, editors, *Numerical Methods for Fluid Dynamics*, pp. 273–285, New York, 1982. Academic.

Table 1. The maximum and average magnitudes of dimensionless spurious currents and pressure jumps at $t = 90$, for a static drop with a radius of 0.25 centered at (0.5,0.5) in a 1×1 domain, using the standard CSF [1] and consistent CSF [5] models. $\Delta x = \Delta y = 1/128$, $\rho_1 = \rho_2 = 10^3$, $\mu_1 = \mu_2 = 5 \times 10^{-2}$, $\sigma = 0.1$, $\Delta t = 0.015$, $\Delta P_{exact} = 0.4$.

	$|\vec{U}\mu/\sigma|_{\max}$	$|\vec{U}\mu/\sigma|_{\text{ave.}}$	$\Delta P_{partial}$	ΔP_{total}	ΔP_{max}
Standard CSF	1.43×10^{-3}	2.1×10^{-5}	0.4008	0.3964	0.5677
Consistent CSF	9.8×10^{-5}	4.0×10^{-6}	0.4008	0.3964	0.4088

Table 2. The maximum and average magnitude of dimensionless spurious currents and pressure jumps at $t = 90$, in a static drop with a radius of 0.25 centered at (0.5,0.5) in a 1×1 domain. Results are of the implicit surface tension model, using (a) the backward Euler scheme (Eq. (15)) and (b) the Crank-Nicolson scheme (Eq. (16)), at different timesteps. $\Delta x = \Delta y = 1/128$, $\rho_1 = \rho_2 = 10^3$, $\mu_1 = \mu_2 = 5 \times 10^{-2}$, $\sigma = 0.1$, $\Delta t_{ST} = 0.03$, $\Delta P_{exact} = 0.4$.

(a)

Δt	$|\vec{U}\mu/\sigma|_{\max}$	$|\vec{U}\mu/\sigma|_{\text{ave.}}$	$\Delta P_{partial}$	ΔP_{total}	ΔP_{max}
0.015	5.30×10^{-4}	7.35×10^{-5}	0.4248	0.4178	0.5505
0.03	1.26×10^{-3}	1.91×10^{-4}	0.3798	0.3767	0.4608
0.06	2.35×10^{-3}	3.83×10^{-4}	0.3661	0.3613	0.4263
0.12	3.29×10^{-3}	5.55×10^{-4}	0.3616	0.3538	0.4397
0.18	3.73×10^{-3}	6.40×10^{-4}	0.3183	0.3091	0.3994

(b)

Δt	$|\vec{U}\mu/\sigma|_{\max}$	$|\vec{U}\mu/\sigma|_{\text{ave.}}$	$\Delta P_{partial}$	ΔP_{total}	ΔP_{max}
0.015	4.59×10^{-4}	6.15×10^{-5}	0.4072	0.4020	0.5218
0.03	1.11×10^{-3}	1.64×10^{-4}	0.3847	0.3806	0.4702
0.06	2.10×10^{-3}	3.38×10^{-4}	0.3848	0.3789	0.4451
0.12	3.04×10^{-3}	5.10×10^{-5}	0.3660	0.3584	0.4387
0.18	3.44×10^{-3}	5.85×10^{-4}	0.3428	0.3346	0.4182
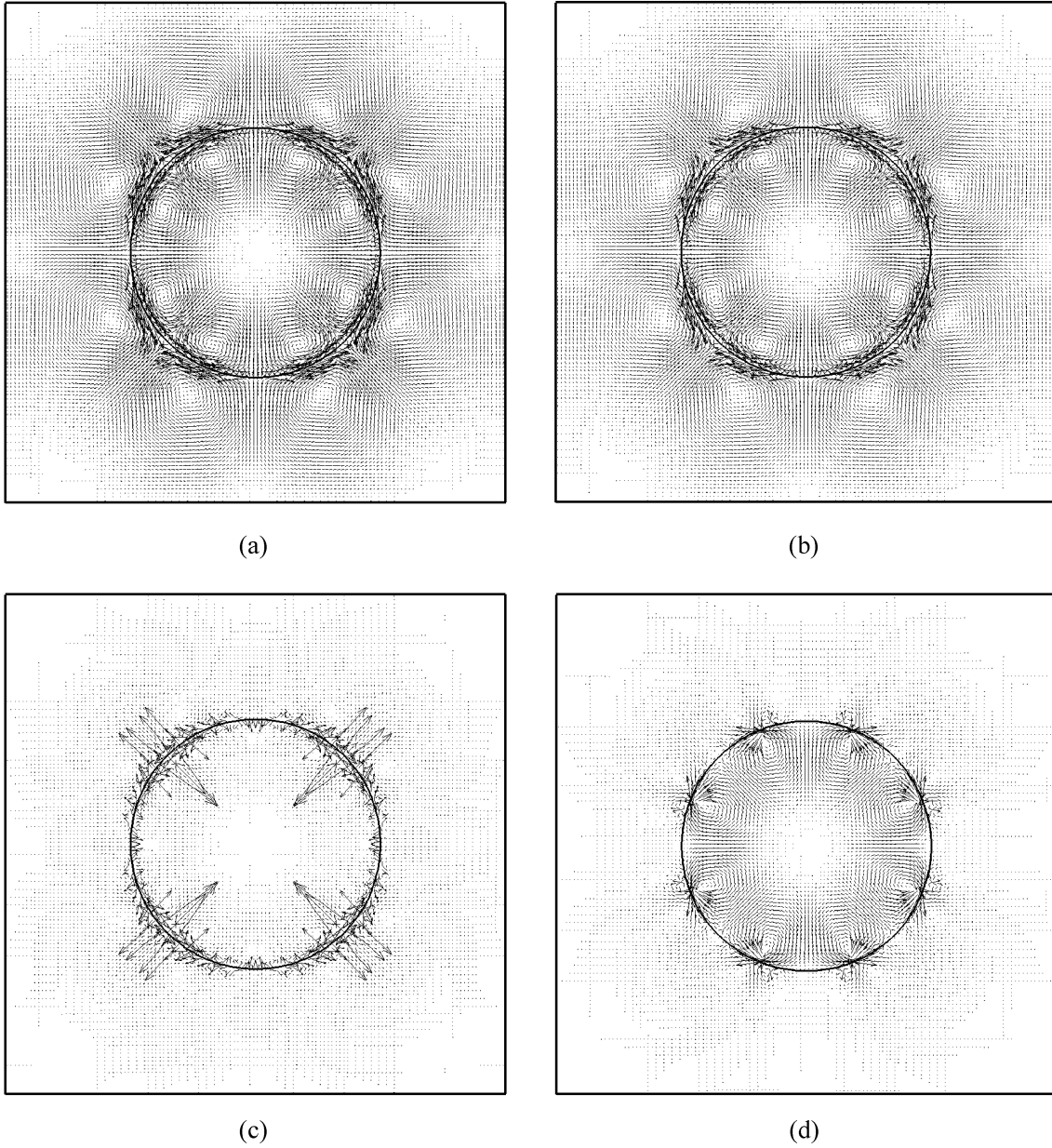
Figure 1. The spurious currents at $t = 90$ in a static drop with a radius of 0.25 centered at (0.5,0.5) in a 1×1 domain. Results are of the implicit surface tension model, using (a) the backward Euler scheme and (b) the Crank-Nicolson scheme. Explicit results are of (c) the standard CSF model and (d) the consistent CSF model (velocities magnified six times). $\Delta x = \Delta y = 1/128$, $\rho_1 = \rho_2 = 10^3$, $\mu_1 = \mu_2 = 5 \times 10^{-2}$, $\sigma = 0.1$, $\Delta t = 0.015$

$\Delta t = 0.006$

(a)   (b)   (c)   (d)

$\Delta t = 0.012$

(a)   (b)   (c)   (d)
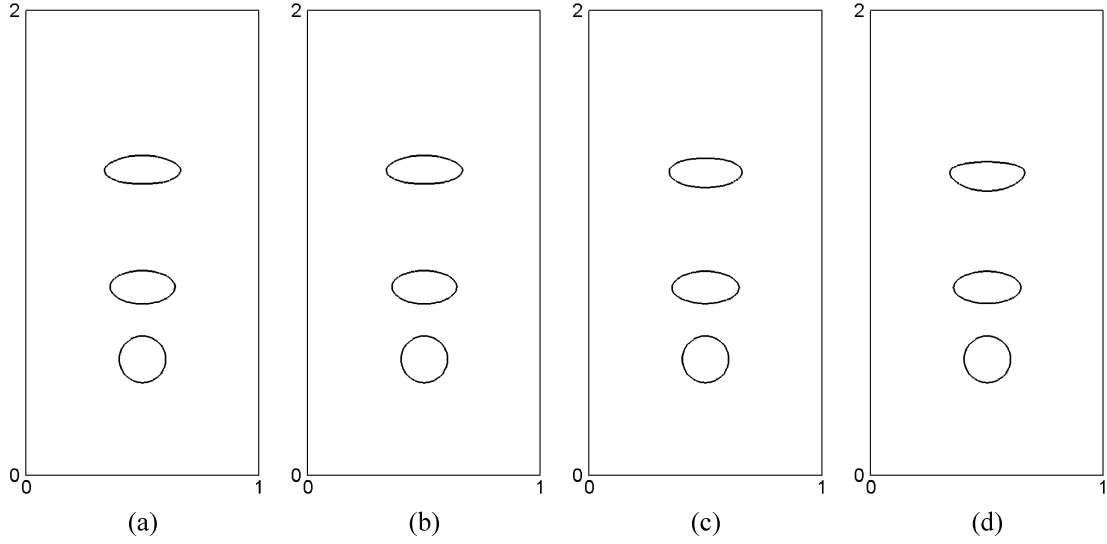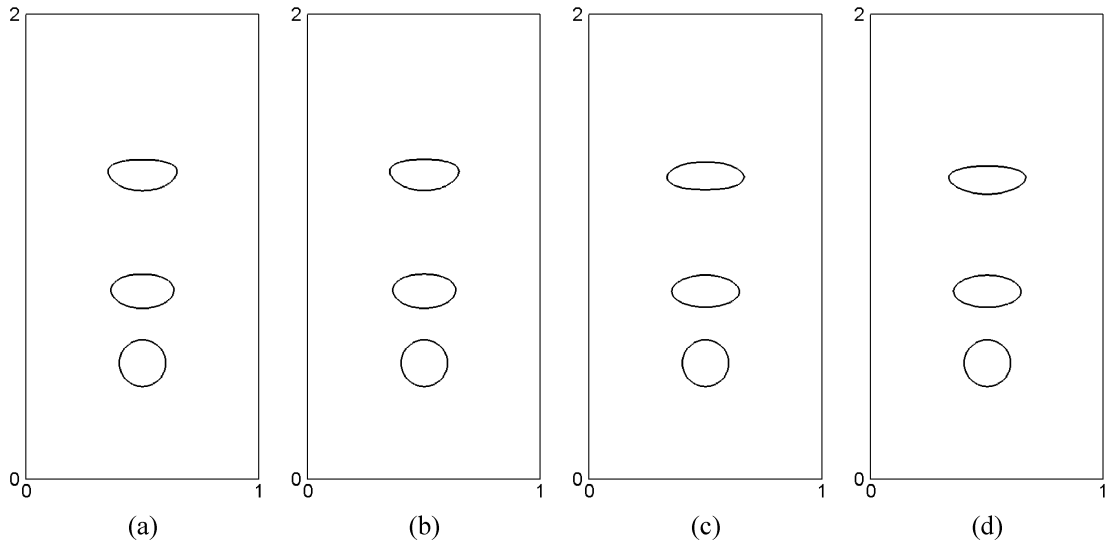
Figure 2. Interface shape as a bubble (fluid 1) rises in fluid 2 due to buoyancy forces. The implicit surface tension model is combined with (a) the backward Euler scheme and (b) the Crank-Nicolson scheme. Explicit results are of (c) the standard CSF model and (d) the consistent CSF model. $\rho_1 = 500$, $\rho_2 = 1000$, $\mu_1 = \mu_2 = 10^{-2}$, $\sigma = 0.1$, $g = -9.81 \times 10^{-3}$, $\Delta x = \Delta y = 1/128$, $\Delta t_{ST} = 0.024$.
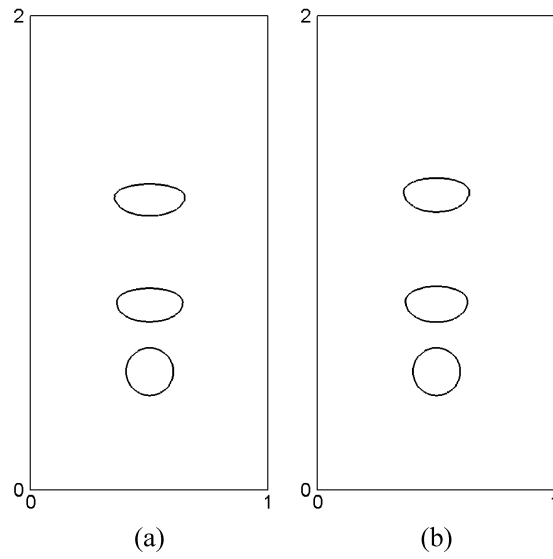
Figure 3. Interface shape as a bubble (fluid 1) rises in fluid 2 due to buoyancy forces. The implicit surface tension model is combined with (a) the backward Euler scheme and (b) the Crank-Nicolson scheme. $\Delta t = 0.12$, $\rho_1 = 500$, $\rho_2 = 1000$, $\mu_1 = \mu_2 = 10^{-2}$, $\sigma = 0.1$, $g = -9.81 \times 10^{-3}$, $\Delta x = \Delta y = 1/128$, $\Delta t_{ST} = 0.024$.